Multiexposure Image Fusion Using Homomorphic Filtering and Detail Enhancement

Hui-Chun Tsai Jin-Jang Leou Han-Hui Hsiao

Department of Computer Science and Information Engineering
National Chung Cheng University
Chiayi 621, Taiwan
{thc100m, jjleou, hhh95p}@cs.ccu.edu.tw

***Abstract*—In this study, a multiexposure image fusion approach using homomorphic filtering and detail enhancement is proposed. First, the *N* input low dynamic range (LDR) RGB color images are transformed into the HSI color space. Intensity enhancement is achieved by homomorphic filtering, gamma correction is used to compensate the nonlinear response of display devices, and "cross-image" median filtering is used to generate the reference intensity image. Guided filtering and weighted least squares (WLS) optimization are used to perform local and global detail extractions on the *N* processed LDR images, respectively. The *N* weighting maps of the *N* processed LDR images are estimated by spatial and cross-image consistencies and then refined by cross bilateral filtering. Finally, the multiresulution spline based scheme is used to perform multiexposure image fusion. Based on the experimental results obtained in this study, the performance of the proposed approach is better than those of four comparison approaches.**

Keywords-low dynamic range (LDR) image; high dynamic range (HDR) image; tone mapping; homomorphic filtering; multiexposure image fusion

I. INTRODUCTION

In the last decade, image fusion has been employed in different application areas [1-2]. Image sensors usually have a limited dynamic range and a low dynamic range (LDR) image usually contains some under-exposed or over-exposed regions. Additionally, a natural scene usually contains high dynamic range (HDR) contents. To cope with this problem, a series of LDR images with different exposures can be fused to obtain an HDR image, which will be displayed on LDR devices. There are two main types of HDR imaging, namely, typical HDR imaging and multiexposure image fusion [3].

HDR imaging consists of two main steps: HDR reconstruction and tone mapping. First, HDR reconstruction techniques [4] usually recover the camera response function (CRF) and combine the radiance maps via a weighting function from a series of LDR images. Second, tone mapping is to compress the dynamic range of HDR images in order to display on LDR devices. Existing tone mapping approaches can be classified into global and local operators [5-7].

Compared to HDR reconstruction, multiexposure image fusion usually consists of two steps: selection and blending [8]. "Selection" decides the best representative regions and exposures among all the input LDR images via assigning weights to the pixels of each LDR image. For blending, the selected regions from LDR images are fused according to their weights individually.

Multiexposure image fusion is similar to alpha blending [9]. Li, Zheng, and Rahardja [10] introduced a new quadratic optimization based image fusion approach. In [3], a mostly detailed LDR image is synthesized directly from input LDR images by solving different optimization problems. Song et al. [11] proposed a probabilistic model to preserve the calculated image luminance levels and suppress reversals in image luminance gradients.

On the other hand, in Mertens et al. [1], a weight for a pixel is determined by three quality measures: contrast, saturation, and well-exposedness. All LDR images are blended at multiple scales by using the Laplacian and Gaussian pyramidal image decompositions. Gu et al. [12] modified the gradient field iteratively with twice average filtering and nonlinearly compressing in multi-scales. Fused gradient field is derived from the structure tensor of LDR images based on multi-dimensional Riemannian geometry. Zhang and Cham [13] used the gradient information to accomplish multiexposure image composition in both static and dynamic scenes. Zhang and Cham [14] also proposed a multiexposure image fusion approach for both static and dynamic scenes using both temporal consistency and spatial consistency. Zeev et al. [15] introduced a new way to construct edge-preserving multi-scale image decompositions, based on weighted least squares (WLS) optimization.

The paper is organized as follows. The proposed multiexposure image fusion approach is described in Section 2. Experimental results are addressed in Section 3, followed by concluding remarks.

II. PROPOSED APPROACH

A. System Architecture

As shown in Fig. 1, the proposed multiexposure image fusion approach for static scenes contains six stages. First, the *N* input LDR color images are transformed from the RGB color space into the hue, saturation, and intensity (HSI) color space so that the intensity and color (hue and saturation) components can be separately processed. Intensity enhancement is achieved by homomorphic filtering in the frequency domain and gamma correction [16] is used to

 ISBN: 978-1-61208-320-9

compensate the nonlinear response of display devices. To eliminate under-exposed or over-exposed regions in LDR images, the "cross-image" median filter is used to generate the reference intensity image. The guided filter [7] and weighted least squares (WLS) optimization [15] are used to perform local and global detail extractions on the *N* processed LDR images with gamma correction, respectively. Based on the reference intensity image, spatial consistency and cross-image consistency involving five consistency measures are computed to estimate the *N* weighting maps of the *N* processed LDR images with gamma correction. The cross bilateral filter is used to refine the *N* weighting maps. Finally, the multiresulution spline based scheme [17] is used to perform multiexposure image fusion and generate the final HDR image.

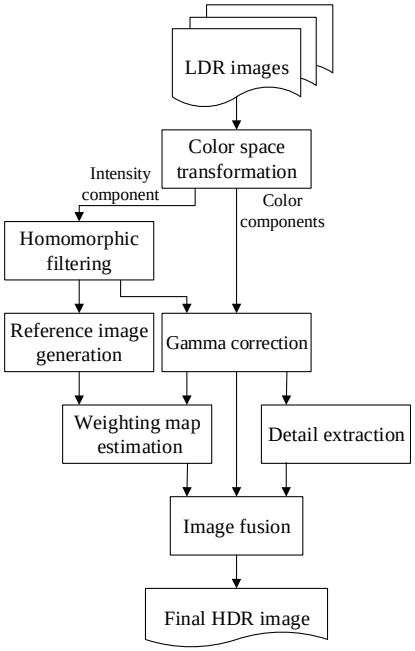

Figure 1. The framework of the proposed approach.

B. Homomorphic filtering

In this study, considering nonlinear intensity perception of the human visual system (HVS), the homomorphic filter is used to perform intensity enhancement in the frequency domain. $I_i^n(x,y)$ denotes the intensity of pixel (x,y) in the *n*-th input LDR image, $I_{i,H}^n(x,y)$ denotes the intensity of pixel (x,y) in the *n*-th homomorphic filtered image, and $H(u,v)$ is the transfer function of the homomorphic filter. The homomorphic filter processes the illumination and reflection components separately in the frequency domain (u,v) via the logarithm function. Here, $H(u,v)$ is a modified Gaussian highpass filter defined as

$$H(u,v) = (r_H - r_L) \cdot [1 - e^{-c(D^2(u,v)/D_0^2)}] + r_L, \quad (1)$$

where the constant *c* controls the sharpness of the transition slop of the filter function between r_L and r_H, D_0 is a positive constant, and $D^2(u,v)$ is the distance between a point (u,v) and the center $(W/2,H/2)$ of the frequency rectangle. Here, r_L, r_H, and *c*, are empirically set to 0, 1, and 1, respectively.

C. Gamma Correction

Gamma correction [16] is used to compensate the nonlinear response of display devices, which is defined as

$$I_C^n = (\frac{I_{C_{in}}^n}{L_{in}})^s \times L_{out}, \qquad C = R,G,B, \quad (2)$$

where *s* denotes the gamma correction coefficient in the range [0,1], $I_{C_{in}}^n$ and I_C^n are the color components of the *n*-th LDR image and the *n*-th processed LDR image with gamma correction, respectively, and L_{in} and L_{out} denote the luminances of I^n and I_H^n (the *n*-th homomorphic filtered LDR color image), respectively.

D. Reference Intensity Image Generation

In this study, the reference intensity image is generated by performing cross-image median filtering over the *N* homomorphic filtered LDR images to exclude under-exposed or over-exposed regions in the *N* input LDR images. Cross-image median filtering is performed in a pixel-by-pixel manner over the *N* homomorphic filtered LDR images to generate the "median" image of $I_H^n(x,y)$, $n = 1,2,\ldots,N$, as the reference intensity image, i.e.,

$$I_R(x,y) = \text{median}(I_H^1(x,y), I_H^2(x,y), \ldots, I_H^N(x,y)), \quad (3)$$

where $I_R(x,y)$ denotes pixel (x,y) of the reference intensity image and *N* is the number of homomorphic filtered LDR images.

E. Detail Extraction

Edge-preserving filters, such as the bilateral filter [18], weighted least squares optimization [15], and the guided filter [7], will not blur strong edges (without ringing artifacts) in the decomposition process. Using edge-preserving filtering, detail extraction is to decompose each processed LDR image with gamma correction into two (base and detail) layers and use the detail layer to compensate image details.

1) Local detail extraction

In this study, the guided filter [7], an edge-preserving filter, is used to decompose each processed LDR image with gamma correction into a base layer and a detail layer, i.e.,

$$I_C = I_L + \hat{I}_L, \quad (4)$$

where I_L and $\hat{I}_L$ denote the base and detail layers, respectively. Here, the guided filter is applied to the three (R, G, B) color component images when edges or fine details are not discriminative in a single color component image. It is assumed that the filtering output I_L is a linear

transformation of the guidance image I_C in a local window Ω centered at pixel *k*, i.e.,

$$I_L^k = a_k^T I_C^k + b_k, \quad (5)$$

where Ω is a 3×3 sliding window, I_L^k and I_C^k denote the 3×3 pixels of I_L and I_C in window Ω, T denotes the transpose operator, and a_k and b_k are two matrices of constants in window Ω, which can be directly estimated by linear regression as

$$a_k = (\mathbf{\Sigma}_k + \varepsilon\mathbf{U})^{-1}(\frac{1}{|\Omega|}\sum_{q\in\Omega} I_C^k P^k - \mu_k \overline{P}_k \mathbf{U}), \quad (6)$$

$$b_k = \overline{P}_k \mathbf{U} - a_k^T \mu_k, \quad (7)$$

where P is the input image, P^k denotes the 3×3 pixels of P in window Ω, $\overline{P}_k$ is the mean of the 3×3 pixels of P in window Ω, μ_k is the mean of the guidance image I_C in window Ω, $|\Omega|$ is the number of pixels in window Ω, ε is a parameter empirically set to 0.16, $\mathbf{\Sigma}_k$ is the 3×3 covariance matrix of the guidance image I_C in window Ω, and $\mathbf{U}$ is the 3×3 identity matrix.

2) Global detail extraction

In this study, WLS optimization [15] is used to decompose each processed LDR image with gamma correction and extract global details. Using matrix notation, we have

$$(\mathbf{I}_G - \mathbf{I}_C)^T(\mathbf{I}_G - \mathbf{I}_C) + \lambda(\mathbf{I}_G^T D_x^T \mathbf{A}_x D_x \mathbf{I}_G + \mathbf{I}_G^T D_y^T \mathbf{A}_y D_y \mathbf{I}_G), \quad (8)$$

where $\mathbf{A}_x$ and $\mathbf{A}_y$ are two diagonal matrices containing the smoothness weights $a_x(I_C)$ and $a_y(I_C)$, respectively, and matrices D_x and D_y are two discrete differentiation operators. The vector $\mathbf{I}_G$ minimizing (8) can be uniquely determined as the solution of

$$\mathbf{I}_C = \mathbf{I}_G(\mathbf{U} + \lambda(D_x^T \mathbf{A}_x D_x + D_y^T \mathbf{A}_y D_y)), \quad (9)$$

where $\mathbf{U}$ is the identity matrix.

F. Weighting Map Estimation and Refinement

For multiexposure image fusion, weighting map estimation is used to form the desired HDR image by keeping only the "best" regions (parts) in input LDR images. Weighting maps are determined by giving weights to the pixels of all LDR images. Here, two quality measures of spatial and cross-image consistency are used to estimate the weighting map of each processed LDR image with gamma correction, which is then refined by the cross bilateral filter.

1) Weighting map estimation of spatial consistency

In this study, four image quality measures of spatial consistency, namely, contrast, saturation, well-exposedness, and saliency, are used to estimate the weighting map of each processed LDR image with gamma correction. Three quality measures of spatial consistency, namely, contrast, saturation, and well-exposedness [1], are defined as

$$W_{\text{contrast}}^n(p) = \left|L(I_C^n(p))\right|, \quad (10)$$

$$W_{\text{saturation}}^n(p) = \sqrt{\frac{\sum_{i\in\{R,G,B\}}(I_{C_i}^n(p) - avg(I_C^n(p)))^2}{3}}, \quad (11)$$

$$W_{\text{exposed}}^n(p) = \exp(-\frac{(I_C^n - 0.5)^2}{2\sigma^2}), \quad (12)$$

where p denotes a pixel in the *n*-th processed LDR image with gamma correction, $|\cdot|$ denotes the absolute value, $L(\cdot)$ is a Laplacian filter with window size 3×3, $avg(\cdot)$ denotes the average of the RGB color components, and σ is empirically set to 0.2. The fourth quality measure of spatial consistency is saliency [4]. First, Laplacian filtering is applied to each processed LDR image with gamma correction to obtain the corresponding high-pass image H^n. Then, the local average of the absolute value of H^n is used to construct the saliency map W_{saliency}^n of H^n, which is computed as

$$W_{\text{saliency}}^n(p) = \left|H^n(p)\right| * G_{\sigma_g}(p), \quad (13)$$

where $H^n(p) = I_C^n(p) * L(p)$, $G_{\sigma_g}(\cdot)$ is a Gaussian filter of size 11×11, the standard derivation σ_g is empirically set to 5, and $*$ is the convolution operator. As a summery, the weighting map of spatial consistency is determined as

$$W_{spatial}^n(p) = W_{contrast}^n(p) \times W_{saturation}^n(p) \times W_{exposed}^n(p) \times W_{saliency}^n(p). \quad (14)$$

2) Weighting map estimation of cross-image consistency

Zhang and Cham [14] found that the gradient directions of the pixels in well-exposed regions are stable in different exposures. Therefore, the weighting map of cross-image consistency can be estimated by measuring gradient direction changes between each processed LDR image with gamma correction and the reference intensity image. Here, the first derivatives of a 2-D Gaussian function in *x* and *y* directions are used to extract the gradient information as

$$\theta^n(x,y) = \arctan(\frac{I_C^n(x,y) * \frac{\partial}{\partial y} G_{\sigma_d}(x,y)}{I_C^n(x,y) * \frac{\partial}{\partial x} G_{\sigma_d}(x,y)}), \quad (15)$$

where $I_C^n(x,y)$ denotes pixel (x,y) in the *n*-th processed LDR image with gamma correction and the standard derivation σ_d is empirically set to 0.5. The weighting map of cross-image consistency is estimated as the 1-D Gaussian function of the difference between $\theta^n(x,y)$ and that $\theta^{ref}(x,y)$ of the reference intensity image, i.e.,

$$W_{temporal}^n = \exp(\frac{-(\theta^n(x,y) - \theta^{ref}(x,y))^2}{2\sigma_t^2}), \quad (16)$$

 ISBN: 978-1-61208-320-9

where σ_t controls the influence of gradient direction changes and σ_t is set adaptively to the exposure quality of the reference intensity image as

$$\sigma_t(x,y)=\begin{cases}\alpha, 1-\gamma < I_R(x,y) < \gamma,\\ \beta, \text{otherwise},\end{cases} \quad (17)$$

where the well-exposed range is $[1-\gamma,\gamma]$ with the image range normalized to $[0,1]$. Here, α controls the influence of gradient direction changes detected based on the well-exposed pixels of the reference intensity image and $\beta(\geq\alpha)$ is used to reduce the influence of the detected gradient direction changes. In this study, the three parameters α, β, and γ are empirically set to 0.02, 0.9, and 0.9, respectively.

3) Weighting map refinement

The initial weighting map directly estimated as

$$W^n_{initial}=W^n_{spatial}\times W^n_{temporal}, \quad (18)$$

may be noisy. To cope with this problem, a cross bilateral filter based refinement [19-20] is employed so that neighboring pixels having similar intensities will have similar weight values, i.e.,

$$W^n_{final}(p)=\frac{\sum_{q\in\Omega} g_{\sigma_s}(\|p-q\|)g_{\sigma_r}(|I^n_C(p)-I^n_C(q)|)W^n_{initial}(q)}{\sum_{q\in\Omega} g_{\sigma_s}(\|p-q\|)g_{\sigma_r}(|I^n_C(p)-I^n_C(q)|)}, \quad (19)$$

where p is a pixel in the n-th weighting map, Ω is a 3×3 sliding window centered at p, and q is a pixel in window Ω. Here, the standard derivations σ_s and σ_t are empirically set to 5 and 5, respectively.

G. Image Fusion

Based on the N weighting maps of the N processed LDR images with gamma correction, a composite image is generated by fusing N processed LDR images with gamma correction. Using the multiresolution spline based scheme [17] to achieve seamless image fusion, the final HDR image I_F is obtained by integrating the composite image and the extracted detail image $I_{detail}=\{\hat{I}^1_L,\ldots,\hat{I}^n_L,\hat{I}^1_G,\ldots,\hat{I}^n_G\}$ as

$$I_F=\frac{\sum_{n=1}^{N} L\{I^n_C\}G\{W^n_{final}\}}{\sum_{n=1}^{N} G\{W^n_{final}\}+\xi}\cdot\exp(\max(I_{detail})), \quad (20)$$

where $L\{\cdot\}$ and $G\{\cdot\}$ denote the Laplacian and Gaussian pyramids, respectively, and ξ is a small constant to avoid singularity.

III. Experimental Results

In this study, the proposed approach is implemented using Matlab 7.10.0 (R2010a) on Intel Core i7-2700K CPU 3.5GHz-Microsoft Windows 7 platform with 8GB main memory. To evaluate the effectiveness of the proposed approach, four comparison approaches are employed, where the source codes of Mertens et al.'s approach [1] and Shen et al.'s approach [3] are directly employed, whereas and Zhang and Cham's approach [14] and Li et al.'s approach [10] are implemented in this study. Here, nineteen LDR image sequences with different numbers of LDR images are employed.

In this study, four objective image quality measures, namely, the structural similarity (SSIM) index [21] , the saturation, the blind image quality index (BIQI) [22], and the naturalness image quality evaluator (NIQE) [23], are employed. In terms of the SSIM index, saturation index, BIQI, and NIQE, the performance comparisons between the four comparison approaches and the proposed approach for the nineteen LDR image sequences are listed in Tables I~IV, respectively. The average performances of the proposed approach are better than those of four comparison approaches. To perform subjective evaluation, subjective scores, i.e., 1 (worst) up to 10 (best), are collected from eighteen people. Here, the final images of multiexposure image fusion of each LDR image sequence are shown on an EIZO LCD color monitor (S2402W) periodically (three seconds per image) and each viewer gives his subjective scores for different final images of each LDR image sequence. The subjective performance comparisons between the four comparison approaches and the proposed approach for the nineteen LDR image sequences are shown in Table V. As two illustrated experimental results shown in Figs. 2 and 3, the overall image quality of the final images of multiexposure image fusion of the proposed approach is better than those of the four comparison approaches. In Fig. 2, more texture details of windows are persevered in the final image of the proposed approach, whereas in Fig. 3, the contrast of books in the final image of the proposed approach is better than those of the four comparison approaches.

IV. Concluding Remarks

In this study, a multiexposure image fusion approach using homomorphic filtering and detail enhancement is proposed. Based on the experimental results obtained in this study, several observations can be found. (1) Based on Tables I~IV, on the average, the objective performance measures, namely, SSIM, saturation, BIQI, and NIQE, of the proposed approach are better than those of the four comparison approaches. (2) Based on Table V, the subjective evaluation of the final HDR images of the proposed approach is better than those of the four comparison approaches. (3) Based on Figs. 2-3, the final HDR images of the proposed approach are indeed better than those of four comparison approaches.

Acknowledgment

The work was supported in part by National Science Council, Taiwan, Republic of China under Grants NSC 102-2221-E-194-028-MY2 and NSC 102-2221-E-194-041-MY3.

References

[1] T. Mertens, J. Kautz, and F. V. Reeth, "Exposure fusion: a simple and practical alternative to high dynamic range photography," Computer Graphics Forum, vol. 28, no. 1, pp. 161-171, 2009.

 ISBN: 978-1-61208-320-9

[2] S. Li,. X. Kang, and J. Hu, "Image fusion with guided filtering," IEEE Trans. on Image Processing, vol. 22, no. 7, pp. 2864-2875, July 2013.

[3] R. Shen, I. Cheng, J. Shi, and A. Basu, "Generalized random walks for fusion of multi-exposure images," IEEE Trans. on Image Processing, vol. 20, no. 12, pp. 3634-3646, Dec. 2011.

[4] P. E. Debevec and J. Malik, "Recovering high dynamic range radiance maps from photographs," in Proc. of ACM SIGGRAPH, 1997, pp. 369-378.

[5] J. Duanm, M. Bressan, and C. Dance, "Tone-mapping high dynamic range images by novel histogram adjustment," Pattern Recognition, vol. 43, no. 5, pp. 1847-1862, May 2010.

[6] T. H. Wang, C. W. Fang, M. C. Sung, and J. J. Lien, "Photography enhancement based on the fusion of tone and color mappings in adaptive local region," IEEE Trans. on Image Processing, vol. 19, no. 12, pp. 3089-3105, Dec. 2010.

[7] K. He, J. Sun, and X. Tang, "Guided image filtering," in Proc. of European Conf. on Computer Vision, 2010, pp. 1-14.

[8] T. Kartalov, Z. Ivanovski, and L. Panovski, "Full automated exposure fusion algorithm for mobile platforms," in Proc. of IEEE Int. Conf. on Image Processing, 2011, pp. 361-364.

[9] S. Raman and S. Chaudhuri, "Bilateral filter based compositing for variable exposure photography," in Proc. of Eurographics, 2009, pp. 1-4.

[10] Z. G. Li, J. H. Zheng, and S. Rahardja, "Detail-enhanced exposure fusion," IEEE Trans. on Image Processing, vol. 21, no. 7, pp. 1-6, July 2012.

[11] M. Song, D. Tao, C. Chen, J. Bu, J. Luo, and C. Zhang, "Probabilistic exposure fusion," IEEE Trans. on Image Processing, vol. 21, no. 1, pp. 341-357, Jan. 2012.

[12] B. Gu, W. Li, J. Wong, M. Zhu, and M. Wang, "Gradient field multi-exposure images fusion for high dynamic range image visualization," Journal of Visual Communication and Image Representation, vol. 23, no. 4, pp. 604-610, May 2012.

[13] W. Zhang and W. K. Cham, "Gradient-directed multiexposure composition," IEEE Trans. on Image Processing, vol. 21, no. 4, pp. 2318-2323, April 2012.

[14] W. Zhang and W. K. Cham, "Reference-guided exposure fusion in dynamic scenes," Journal of Visual Communication and Image Representation, vol. 23, no. 3, pp. 467-475, April 2012.

[15] F. Zeev, F. Raanan, L. Dani, and S. Richard, "Edge-preserving decompositions for multi-scale tone and detail manipulation," ACM Trans. on Graphics, vol. 27, no. 3, pp. 1-10, 2008.

[16] J. Tumblin, J. K. Hodgins, and B. K. Guenter, "Two methods for display of high contrast images," ACM Trans. on Graphics, vol. 18, no. 1, pp. 56-94, 1999.

[17] P. J. Burt and E. H. Adelson, "A multiresolution spline with application to image mosaics," ACM Trans. on Graphics, vol. 2, no. 2, pp. 217-236, 1983.

[18] F. Durand and J. Dorsey, "Fast bilateral filtering for the display of high-dynamic-range images," ACM Trans. on Graphics (Proc. of ACM SIGGRAPH 2002), vol. 21, no. 3, pp. 257-266, July 2002.

[19] E. Eisemann and F. Durand, "Flash photography enhancement via intrinisic relighting," ACM Trans. on Graphics, vol. 23, no. 1, pp. 673-678, 2004.

[20] G. Petschnigg, R. Szeliski, M. Agrawala, M. Cohen, H. Hoppe, and K. Toyama, "Digital photography with flash and no-flash image pairs," ACM Trans. on Graphics, vol. 23, no. 1, pp. 664-672, 2004.

[21] Z. Wang, A. C. Bovik, H. R. Sheikh, and E. P. Simoncelli, "Image qulaity assessment: from error visibility to structural similarity," IEEE Trans. on Image Processing, vol. 13, no. 4, pp. 600-612, April 2004.

[22] A. K. Moorthy and A. C. Bovik, "A two-step framework for constructing blind image quality indices," IEEE Signal Processing Letters, vol. 17, no. 5, pp. 513-516, May 2010.

[23] A. Mittal, R. Soundararajan, and A. C. Bovik, "Making a completely blind image quality analyzer," IEEE Signal Processing Letters, vol. 22, no. 3, pp. 209-212, March 2013.

(a) (b) (c) (d) (e)

Figure 2. The final images of multiexposure image fusion of the "Church" LDR image sequence: (a) Mertens et al. [1]; (b) Shen et al. [3]; (c) Zhang and Cham [14]; (d) Li et al. [10]; (e) proposed.

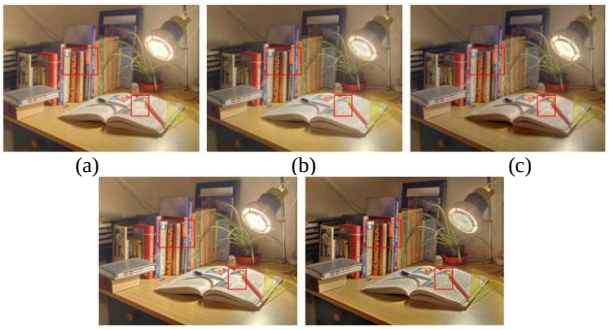

(a) (b) (c) (d) (e)

Figure 3. The final images of multiexposure image fusion of the "Desk Lamp1" LDR image sequence: (a) Mertens et al. [1]; (b) Shen et al. [3]; (c) Zhang and Cham [14]; (d) Li et al. [10]; (e) proposed.

TABLE I. IN TERMS OF SSIM, PERFORMANCE COMPARISONS BETWEEN THE FOUR COMPARISON APPROACHES AND THE PROPOSED APPROACH FOR THE NINETEEN LDR IMAGE SEQUENCES

LDR image sequences	Mertens et al. [1]	Shen et al. [3]	Zhang and Cham [14]	Li et al. [10]	Proposed
Aloe	68.2%	70.0%	71.0%	61.2%	**89.7%**
Ardeshir	76.5%	78.5%	77.6%	75.1%	**84.3%**
Belgium	40.6%	47.6%	46.6%	44.6%	**63.4%**
Bridge	80.1%	82.6%	77.9%	79.2%	**86.4%**
Church	70.3%	70.7%	**70.9%**	63.6%	67.7%
Desk Lamp1	80.8%	**81.6%**	80.5%	76.0%	79.6%
Desk Lamp2	77.6%	**79.0%**	72.5%	72.8%	75.1%
Flower8	63.5%	64.7%	63.5%	60.0%	**72.8%**
GrandCanal	62.2%	64.2%	61.5%	59.3%	**73.6%**
Hall	80.9%	**81.7%**	80.8%	79.4%	81.6%
HDRLab3	67.4%	67.2%	66.8%	66.5%	**80.4%**
House	42.1%	43.2%	41.9%	40.4%	**51.1%**
Kitchen	68.4%	71.2%	68.2%	64.5%	**76.8%**
Landscape	75.8%	76.4%	72.0%	74.0%	**85.4%**
Lighthouse	71.1%	72.8%	70.9%	68.0%	**80.5%**
Mountain	80.5%	**81.9%**	78.7%	76.1%	78.7%
Sofa	61.2%	61.4%	62.1%	57.5%	**64.1%**
Tree	70.1%	70.0%	**70.4%**	67.0%	65.0%
Wall	59.9%	61.1%	59.3%	59.4%	**67.4%**
Average	68.6%	69.8%	68.1%	65.5%	**74.9%**

TABLE II. IN TERMS OF SATURATION, PERFORMANCE COMPARISONS BETWEEN THE FOUR COMPARISON APPROACHES AND THE PROPOSED APPROACH FOR THE NINETEEN LDR IMAGE SEQUENCES

LDR image sequences	Mertens et al. [1]	Shen et al. [3]	Zhang and Cham [14]	Li et al. [10]	Proposed
Aloe	0.33	0.31	0.38	0.33	**0.45**
Ardeshir	0.38	0.32	0.40	0.38	**0.40**
Belgium	0.30	0.24	**0.33**	0.30	0.32
Bridge	0.13	0.12	0.14	0.13	**0.17**
Church	0.64	0.60	0.65	0.64	**0.69**
Desk Lamp1	0.39	0.38	0.39	0.39	**0.44**
Desk Lamp2	0.28	0.26	0.24	0.28	**0.31**
Flower8	0.28	0.24	0.27	0.28	**0.32**
GrandCanal	0.22	0.14	0.22	0.22	**0.25**
Hall	0.30	0.26	0.31	0.29	**0.33**
HDRLab3	0.27	0.24	**0.33**	0.27	0.32
House	0.33	0.25	0.35	0.33	**0.36**
Kitchen	0.46	0.39	0.47	0.46	**0.53**
Landscape	0.18	0.17	0.16	0.18	**0.22**
Lighthouse	0.39	0.34	**0.41**	0.39	0.37
Mountain	0.15	0.12	0.15	0.15	**0.18**
Sofa	0.82	0.78	**0.87**	0.81	**0.87**
Tree	0.15	0.13	0.15	0.15	**0.18**
Wall	0.20	0.11	0.19	0.20	0.17
Average	0.33	0.28	0.34	0.32	**0.36**

TABLE III. IN TERMS OF BIQI, PERFORMANCE COMPARISONS BETWEEN THE FOUR COMPARISON APPROACHES AND THE PROPOSED APPROACH FOR THE NINETEEN LDR IMAGE SEQUENCES

LDR image sequences	Mertens et al. [1]	Shen et al. [3]	Zhang and Cham [14]	Li et al. [10]	Proposed
Aloe	57.65	69.12	62.07	39.78	**32.16**
Ardeshir	24.31	29.39	**21.71**	27.41	23.47
Belgium	18.17	28.97	18.14	**12.50**	17.97
Bridge	31.33	32.64	31.53	26.94	**23.14**
Church	26.27	31.60	29.49	21.36	**19.59**
Desk Lamp1	21.97	27.22	27.23	**16.58**	17.33
Desk Lamp2	24.45	27.33	33.38	**16.41**	17.57
Flower8	29.51	33.79	29.76	25.07	**20.49**
GrandCanal	24.47	29.27	24.20	31.19	**23.99**
Hall	**18.09**	29.80	18.45	26.21	27.39
HDRLab3	29.90	30.66	31.22	**25.26**	30.84
House	**27.54**	31.66	27.98	32.78	27.80
Kitchen	26.65	31.42	27.38	22.80	**21.22**
Landscape	26.40	**25.32**	25.59	26.74	27.66
Lighthouse	**11.04**	23.64	11.36	13.57	11.98
Mountain	36.20	41.07	36.66	23.77	**17.10**
Sofa	38.55	39.79	**32.61**	41.20	39.97
Tree	26.06	27.00	27.91	14.06	**13.65**
Wall	23.68	26.71	24.30	24.49	**22.26**
Average	27.48	32.44	28.47	24.64	**22.92**

TABLE IV. IN TERMS OF NIQE, PERFORMANCE COMPARISONS BETWEEN THE FOUR COMPARISON APPROACHES AND THE PROPOSED APPROACH FOR THE NINETEEN LDR IMAGE SEQUENCES

LDR image sequences	Mertens et al. [1]	Shen et al. [3]	Zhang and Cham [14]	Li et al. [10]	Proposed
Aloe	2.99	**2.57**	2.88	2.77	2.83
Ardeshir	3.86	**3.18**	3.38	3.80	3.38
Belgium	2.38	2.45	2.24	2.19	**2.07**
Bridge	2.42	2.42	2.36	2.20	**2.13**
Church	2.09	1.90	**1.77**	1.98	1.86
Desk Lamp1	2.61	2.42	2.53	2.27	**2.25**
Desk Lamp2	2.70	2.54	2.47	2.34	**2.21**
Flower8	1.87	2.02	1.86	**1.65**	1.66
GrandCanal	2.33	2.27	2.27	2.16	**2.08**
Hall	2.49	2.39	2.41	2.39	**2.31**
HDRLab3	2.98	3.21	2.98	**2.57**	2.74
House	2.52	2.52	2.53	**2.33**	2.41
Kitchen	3.08	3.07	2.74	2.86	**2.65**
Landscape	3.06	**2.15**	3.01	2.79	2.63
Lighthouse	3.47	**2.89**	3.44	3.09	3.34
Mountain	2.07	2.14	2.17	**2.03**	2.06
Sofa	3.29	3.13	3.11	3.18	**3.05**
Tree	1.93	1.85	1.87	1.79	**1.75**
Wall	2.55	2.40	**2.15**	2.55	2.29
Average	2.67	2.50	2.54	2.47	**2.40**

TABLE V. IN TERMS OF SUBJECTIVE EVALUATION, PERFORMANCE COMPARISONS BETWEEN THE FOUR COMPARISON APPROACHES AND THE PROPOSED APPROACH FOR THE NINETEEN LDR IMAGE SEQUENCES

LDR image sequences	Mertens et al. [1]	Shen et al. [3]	Zhang and Cham [14]	Li et al. [10]	Proposed
Aloe	5.94	4.72	5.50	7.67	**8.94**
Ardeshir	**8.00**	5.67	5.56	7.33	6.78
Belgium	7.11	5.11	6.89	**7.22**	6.83
Bridge	4.94	6.28	5.78	6.56	**8.89**
Church	6.72	5.33	7.11	6.33	**8.67**
Desk Lamp1	6.44	5.67	5.61	7.11	**9.11**
Desk Lamp2	6.89	5.83	3.44	7.28	**8.22**
Flower8	6.17	5.44	6.00	7.11	**8.64**
GrandCanal	7.33	5.61	7.50	**8.33**	6.17
Hall	7.06	6.11	7.06	7.61	**8.14**
HDRLab3	6.17	5.22	7.28	6.50	**7.89**
House	8.06	5.28	7.28	**8.33**	8.06
Kitchen	7.67	5.28	6.22	7.67	**8.78**
Landscape	7.28	6.06	6.50	**7.89**	7.56
Lighthouse	7.50	5.56	7.22	**8.78**	7.00
Mountain	6.83	5.78	6.67	**8.33**	**8.33**
Sofa	7.50	5.78	6.06	7.17	**8.33**
Tree	5.56	5.61	6.22	7.11	**8.89**
Wall	6.94	6.67	6.39	7.22	**8.61**
Average	6.85	5.63	6.33	7.45	**8.10**

 ISBN: 978-1-61208-320-9